Binary vascular reconstruction from a limited number of cone beam projections

Normand Robert[a)]
Department of Medical Biophysics, Sunnybrook Health Science Centre, University of Toronto, 2075 Bayview Avenue, Room SG06, Toronto, Ontario, M4N 3M5 Canada

Françoise Peyrin
URA CNRS 1216-LTSU BAT-502 INSA Villeurbanne Cedex, France

Martin J. Yaffe
Department of Medical Biophysics, Sunnybrook Health Science Centre, University of Toronto, 2075 Bayview Avenue, Room SG06, Toronto, Ontario, M4N 3M5 Canada

(Received 17 May 1993; resubmitted 18 April 1994; accepted for publication 21 June 1994)

This paper describes a method to perform reconstruction of vascular cross-sectional images from a limited number of x-ray angiographic cone-beam projections. It is assumed that the projection data can be simplified by identifying blood vessels in each angiogram and removing signals due to other structures. Under these conditions, the x-ray attenuation coefficient, μ, can be modeled as a binary variable having a value μ_0 within the vessel and "0" outside. The reconstruction is performed by minimizing a cost function using the method of simulated annealing. In this paper, we demonstrate that the introduction of *a priori* information allows one to reconstruct a sphere and a simulated branched vessel from three views with, respectively, 97% and 93% of voxels having correct values. The addition of a continuity constraint for the reconstruction of the branched vessel resulted in further reduction in the percentage of misplaced voxels. Calculations require from one to six hours of CPU time on a Sun SparcStation 2 computer for the cases investigated here. The effect of noise, "cooling" schedule, and number of views on the reconstruction are examined using simulated vessel projections. Modifications to our approach to accelerate the reconstruction are also discussed.

Key words: angiography, reconstruction, limited-view reconstruction, optimization, simulated annealing

I. INTRODUCTION

Several studies have demonstrated that visual assessment of the dimensions of a lesion from angiograms is subject to considerable inter- and intra-observer variability which can affect decisions on the course of treatment.[1–3] These findings have stimulated the development of computer-aided quantitative approaches to measure vessel dimensions and positions. Such methods are potentially advantageous in that they are not subject to variations in the performance of the human observer.[4–10] In this paper, we will describe a method to perform limited-view divergent (cone–beam) reconstruction of vascular cross sections. The approach used is an extension of a parallel beam binary reconstruction algorithm for two orthogonal views, first proposed by Chang.[11]

Quantitative methods for angiography can be used to determine the cross-sectional area of a selected blood vessel segment.[6] A technique which can also determine the shape of a vessel lumen might provide an important tool in measuring the progression of vascular disease or its regression as a result of therapy. In order to perform this task, an image reconstruction technique must be used. Conventional computed tomography is not well suited for this undertaking since the time required to obtain multiple slices is several seconds. As well, because of the size and spacing of the x-ray detectors, resolution of the CT images is currently insufficient to assess the patency of smaller vessels in which an intervention might be considered. Although an improvement in spatial resolution of CT is possible, it would necessitate a large increase in radiation dose to the patient.

If, as is current in angiography, images are acquired as cone–beam projections using an area detector such as an image intensifier, data for each view can be obtained in a few milliseconds. A full 3D CT reconstruction can be performed from these two-dimensional projections but the number of views required to solve this ill-posed problem would be large. However, if *a priori* information can be introduced, the number of views required to perform an acceptable reconstruction could be significantly reduced and cross-section imaging could be performed using projections obtained with suitably modified angiographic equipment.

A number of approaches have been developed to perform limited view reconstruction.[12–16] These methods yield significant improvements over classical reconstruction methods like filtered back-projection and ART when used with a small number (<8) views. However, in order to depict the shape of a vessel from a limited number of views with even greater accuracy, additional constraints must be added. These constraints are derived from *a priori* information specific to the particular imaging problem and are introduced in order to further restrict the nature of the solutions obtained. One way in which this can be accomplished is to simplify the projection data by identifying the signal due to blood vessels in each projection and removing the signal due to structures other than vessels. This might be achieved by subtracting an image obtained prior to the injection of contrast agent or

a)Tel: (416)480-6100, ext. 3282; Fax: (416) 480-5714, E-mail: robert@srcl.sunnybrook.utoronto.ca

 0094-2405/94/21(12)/1839/13/$1.20 © 1994 Am. Assoc. Phys. Med.

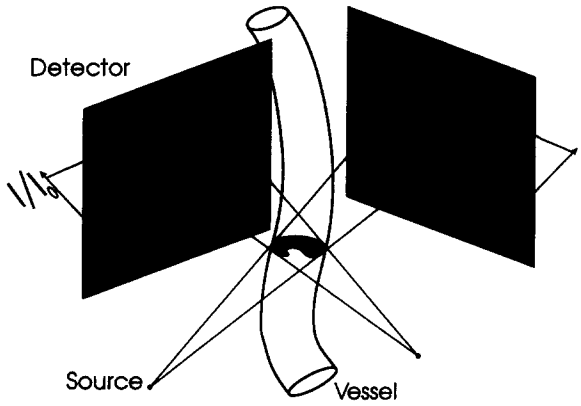

FIG. 1. Diagram depicting how the signal I/I_0 provides information regarding the path length traveled by x-rays through an iodinated vessel along a line joining each detector element to the x-ray source.

possibly by identifying blood vessels, estimating the background signal in their vicinity and using this information to isolate the signal due to the opacified vessels.

If the injection of contrast agent is performed with sufficient vigor to displace blood, the fluid in the arteries will have a uniform composition and if no other signals are present, the incremental x-ray attenuation coefficient due to the presence of the opacified vessel lumen, can be written as

$$\mu(x,y,z)=\begin{cases}\mu_0 & \text{within a vessel}\\ 0 & \text{otherwise}\end{cases}. \tag{1}$$

In order to simplify both this discussion and our simulations, a value of $\mu_0=1$ will be used in the remainder of this paper, i.e., the attenuation coefficient of the vessel will be treated as a binary variable.

We consider an image in which the signal due to attenuation by nonvascular tissue has been removed. Let I_0 be the signal due to x rays interacting with a detector in the absence of any absorber and I be the signal following attenuation of the x rays along a path length t of contrast medium. In the case of a monoenergetic x-ray source and pencil-beam geometry (no scatter contributing to I), the Beer–Lambert relationship allows calculation of the path length as

$$t=-\ln\left(\frac{I}{I_0}\right)\frac{1}{\mu_0}. \tag{2}$$

Binary reconstruction uses such path length information obtained from multiple radiographic views as shown in Fig. 1 to determine the shape of the vessel lumen. However, it is not realistic from a computational point of view to perform binary reconstruction by generating all 2^n distinct objects having n voxels. Chang[11,17,18] and Wang[19] investigated this problem and developed methods to reconstruct a two-dimensional slice from two orthogonal one-dimensional projections. Slump and Gerbrands[20] performed binary reconstruction on orthogonal projections of heart ventricles adding constraints to favor continuity between adjacent slices. Reiber[21] applied these ideas to the reconstruction of coronary arteries. Finally, Van Tran *et al.*[22] performed binary reconstruction of phantoms and of an "*in vitro* heart" using an algorithm in which cross-coordinate moments are obtained based on assumption of connectivity and continuity and inverted to obtain slices of the object.

If additional views are added, it is no longer possible to perform reconstruction in the manner proposed by Chang *et al.* This is because one cannot specify the criteria for the assignment of values to voxels for rays acquired at arbitrary angles, since a given voxel will appear in adjacent ray sums with different weighting coefficients.[23] When values are assigned according to an heuristic rule, as proposed by Crewe[24,25] and Krishnan,[26] we have determined that incorrect assignments of voxel values may occur and that these will not be detected until additional values are assigned and inconsistencies appear. Furthermore, when an inconsistency does appear, it will not be possible to determine which pixel assignment was the cause. Although these methods will not in general satisfy the projection data exactly, Crewe has shown that the reconstruction does resemble the original object from which the projections were generated.

In summary, if we use existing reconstruction methods, we are faced with a dilemma. (1) We can use Chang's algorithm for two orthogonal parallel beam views which provides a reconstruction that will satisfy the projection data exactly if these data are consistent. If the object is complex, several reconstructions will satisfy the projection data and the results obtained will be suboptimal. (2) We can use more views to resolve ambiguities that arise from the reconstruction of complex objects but methods suggested thus far make voxel assignments according to heuristic rules.

The method we propose differs in two respects (1) It incorporates the cone beam geometry encountered in angiography. (2) Since, like our predecessors, we have been unable to find a rule to assign a definite value to a given voxel, we have developed a method where no single voxel assignment is permanent. In other words, the value of a particular voxel may be changed several times during the reconstruction process as is the case in iterative reconstruction methods.

II. MULTIPLE-VIEW CONE–BEAM BINARY RECONSTRUCTION

A. Acquisition geometry and projection operator

Since angiograms are the result of divergent projections of opacified vessels, it is desirable to develop a reconstruction method that will work with two-dimensional cone–beam projections. In addition, this method would be most practically implemented if it were flexible regarding the angular distribution of these views, allowing one to select an acquisition geometry that will minimize the overlap in the projection of vessels. It is also desirable for this approach to function with an arbitrary number of views in order to overcome the ambiguities associated with two view reconstruction when multiple vessels are present.[27]

Figure 2 depicts the acquisition geometry used for binary reconstruction. The origin of the three-dimensional coordinate system is given by the point O. The position of the x-ray source is given by the vector $\mathbf{s}$. The detector lies in a plane normal to the unit vector $\mathbf{n}$ and D is a point that intersects the detector plane which defines the vector $\mathbf{d}=O\mathbf{D}$. The position

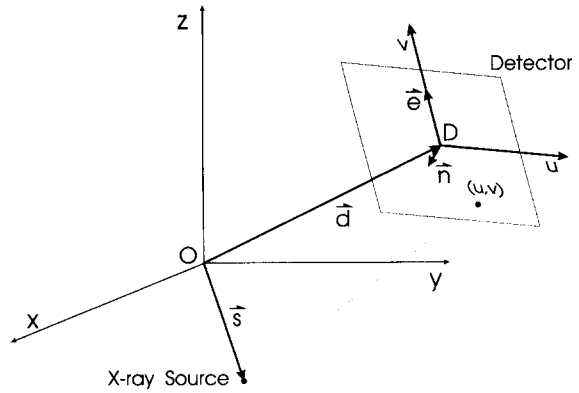

FIG. 2. Acquisition geometry for limited-view cone–beam reconstruction.

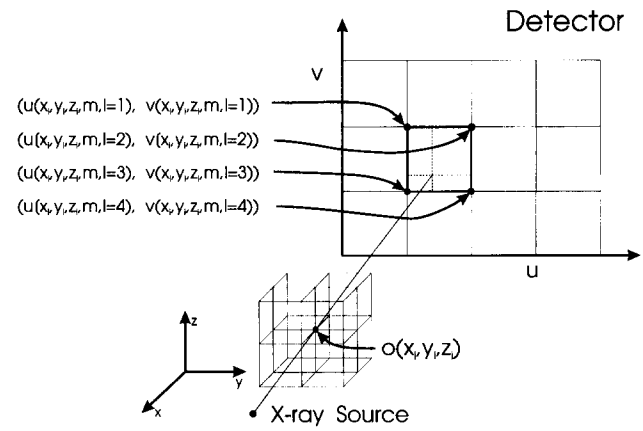

FIG. 3. Diagram depicting how the signal from a single voxel is projected onto $l_{max}=4$ detector elements.

of a point in the detector plane is given in terms of a second coordinate system (u,v) originating at the point D. The v axis is parallel to the unit vector $\mathbf{e}$ while the u axis is parallel to $\mathbf{e}\times\mathbf{n}$. From these definitions, it follows that a ray joining the x-ray source to a point (u_0,v_0) in the detector plane is specific in terms of the parameter q by

$$(x,y,z)=\mathbf{f}q+\mathbf{s}, \tag{3}$$

where $\mathbf{f}$ is a vector such that

$$\mathbf{f}=v\mathbf{e}+u\mathbf{e}\times\mathbf{n}+\mathbf{d}-\mathbf{s}. \tag{4}$$

Knowledge of the acquisition geometry allows one to determine the projection coordinates (u,v) of a point (x,y,z) in the patient by solving for A, B, C in the linear system

$$\begin{aligned} x-s_x&=Ae_x+B(e_yn_z-e_zn_y)+C(d_x-s_x),\\ y-s_y&=Ae_y+B(e_zn_x-e_xn_z)+C(d_y-s_y),\\ z-s_z&=Ae_z+B(e_xn_y-e_yn_x)+C(d_z-s_z), \end{aligned} \tag{5}$$

where $A=vq$, $B=uq$, $C=q$ so that $v=A/C$ and $u=B/C$.

A set of two-dimensional projections through an object having an x-ray attenuation coefficient, $\mu(x,y,z)$, along lines described in Eq. (3) are given by the path integral

$$p_{\mathbf{fs}}(u,v)=\int \mu\left(\frac{\mathbf{f}}{\|\mathbf{f}\|}h+\mathbf{s}\right)dh. \tag{6}$$

In order to perform reconstruction of digital images, we define a discrete projection operator based on Eq. (6). A three-dimensional binary object can be defined as

$$o(x_i,y_i,z_i)=\begin{cases}1 & \text{if voxel } (x_i,y_i,z_i) \text{ is part of the vessel}\\ 0 & \text{otherwise}\end{cases}, \tag{7}$$

where i is an index over all voxels. We define an operator P that projects a discrete binary object composed of voxels to form sets of two-dimensional images denoted by $p(m,u,v)$ such that

$$p(m,u_j,v_j)=P\{o\}(m,u_j,v_j)=P\{o(x_i,y_i,z_i)\}, \tag{8}$$

where (u_j,v_j) are the coordinates of the jth detector element and m is an index indicating the view number. This operation implicitly contains weighting coefficients describing how rays interact with a three-dimensional volume of voxels. We choose a discretization formula given by

$$\begin{aligned} p(m,u_j,v_j)=\sum_{i,l}\ &\delta(u_j-u(x_i,y_i,z_i,m,l))\\ &\times\delta(v_j-v(x_i,y_i,z_i,m,l))\\ &\times o(x_i,y_i,z_i)w(x_iy_i,z_i,m,l), \end{aligned} \tag{9}$$

where

$$\delta(x)=\begin{cases}1 & \text{if } x=0\\ 0 & \text{otherwise}\end{cases} \tag{10}$$

is a discrete delta function.

The expressions $u(x_i,y_i,m,l)$ and $v(x_i,y_i,z_i,m,l)$ provide the positions of all detector elements onto which a voxel located at (x_i,y_i,z_i) will project and are determined by solving the linear system described in Eq. (5) for (u,v) and selecting the detector elements closest to that location. The variable l $(1\leq l\leq l_{max})$ is an index over these detector elements. In this paper, the weighting coefficients are calculated using bilinear interpolation and at most $l_{max}=4$ detector elements are affected by the projection of a given voxel as shown in Fig. 3. The factor $w(x_i,y_i,z_i,m,l)$ weights the contribution of the voxel (x_i,y_i,z_i) to the various detector elements in each view and is normalized so that

$$\sum_{l=1}^{l_{max}} w(x_i,y_i,z_i,m,l)=1 \quad \forall i,m. \tag{11}$$

It is also possible to specify the projection operator in terms of $W(m,u_j,v_j,k)$, a detector-based weighting coefficient where k is an index over all the voxels that interact with a ray from the source to the detector element having coordinates (u_j,v_j). The projection operation can then be written as

$$p(m,u_j,v_j)=\sum_k o(x(m,u_j,v_j,k),y(m,u_j,v_j,k),$$
$$z(m,u_j,v_j,k))W(m,u_j,v_j,k). \quad (12)$$

Equation (12) is a more compact method of expressing the projection operator but Eq. (9) is a more convenient form to use in our approach to solving the binary reconstruction problem.

B. Mask function

If we can identify projections of blood vessels in all the available views, we can specify a volume to which to the reconstruction process can be confined by defining the mask function

$$\text{mask}(x_i,y_i,z_i)=\begin{cases} 0 \quad \text{if} \quad \forall l,m \quad \begin{cases} p[m,u(x_i,y_i,z_i,m,l),v(x_i,y_i,z_i,m,l)]=0 \quad \text{or} \\ \{p[m,u(x_i,y_i,z_i,m,l),v(x_i,y_i,z_i,m,l)]\neq 0 \\ \text{and} \quad w(x_i,y_i,z_i,m,l)=0\} \end{cases} \\ 1 \quad \text{otherwise.} \end{cases} \quad (13)$$

In other words, if none of the projections of a given voxel correspond to a point on the detector that has been identified as being part of the projection of a vessel, then that voxel cannot be part of the vessel and $\text{mask}(x_i,y_i,z_i)=0$. For the remaining voxels, which may be part of the vessel, $\text{mask}(x_i,y_i,z_i)=1$. The mask function provides a key constraint in the reconstruction process since it is used to determine regions in the volume in which the vessel cannot lie. It is often the case that vessels comprise less than 20% of the reconstruction volume, resulting in a correspondingly small fraction of voxels for which the mask equals "1." Since binary reconstruction is only performed on these voxels, computation time and memory requirements can both be markedly reduced.

C. Minimization of a cost function

To reconstruct a vessel, a three-dimensional object satisfying the projection data must be conceived. Let us define $\tilde{o}(x_i,y_i,z_i)$, to be an estimate of the vessel which we are attempting to reconstruct and P as the projection operator defined in Eq. (8). We want to minimize the expression for the "cost"

$$C=\sum_{m,j} g[\Delta p(m,u_j,v_j)], \quad (14)$$

where

$$\Delta p(m,u_j,v_j)=P\{\tilde{o}\}(m,u_j,v_j)-p(m,u_j,v_j) \quad (15)$$

is the difference between the original projection data and the projection of the partial reconstruction and g can be any even, monotonically increasing function [we use $g(\Delta p)=\Delta p^2$] which provides a measure of how closely a projection of $\tilde{o}$ agrees with the original projection set. Our aim is to minimize the cost function subject to constraints imposed by a mask function and "binarity" of the object.

D. Simulated annealing

Iterative reconstruction methods like ART[28] provide solutions that satisfy the projection data in a least square sense, but we found no examples in the literature of constraints such as "binarity" being introduced with these methods. Our experience in this area suggests that when such constraints are added, iterative approaches do not converge toward the correct solution. Therefore, the strategy used has been to transform the reconstruction problem into one of optimization that will allow the introduction of the constraints.

This approach presents some new difficulties, namely, no optimization method has been developed that guarantees the determination of the global minimum of the cost function without performing an exhaustive search. In our case, the number of configurations is far too large to permit such a search for all possible solutions. Therefore, we have adopted the method of "simulated annealing,"[29] which has yielded optimal solutions of problems of very large scale. Figure 4 illustrates the various steps in the reconstruction process including the simulated annealing loop with the aid of a flow diagram.

Using this method, one creates an initial estimate of the vessel, $\tilde{o}$ and calculates the cost function given in Eq. (14). A modification to $\tilde{o}$ is attempted, and the change in cost

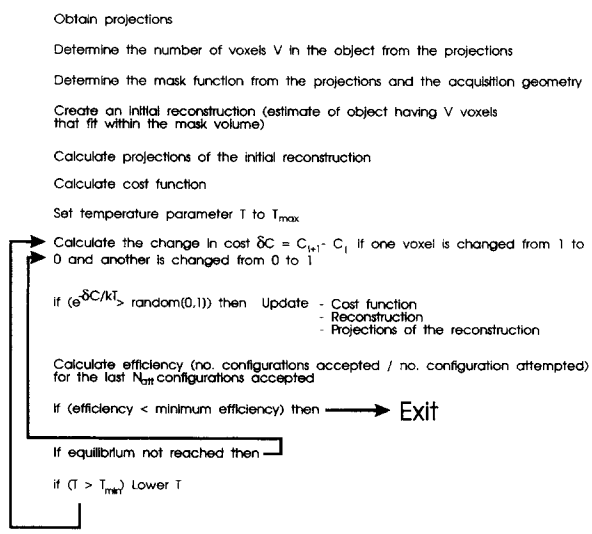

FIG. 4. Flow chart for the reconstruction algorithm.

$\delta C = C_{new} - C_{old}$ is then calculated. The decision to accept or reject this change is made according to the probability function

$$\text{Prob}(\delta C) = \begin{cases} 1 & \text{if} \quad \delta C < 0 \\ e^{-\delta C/kT} & \text{if} \quad \delta C \geq 0 \end{cases} \tag{16}$$

originally proposed by Metropolis.[30] This condition is implemented by accepting a change in configuration if

$$e^{-\delta C/kT} > \text{random}[0, 1], \tag{17}$$

where random[0, 1] is a random number generator producing uniformly distributed values between zero and one. Each attempt to modify $\tilde{o}$ is called an iteration, and each time a modification to $\tilde{o}$ is performed we say that $\tilde{o}$ has taken on a new configuration.

If δC is negative, the new cost is less than the previous one indicating that the modification constitutes an improvement and the new configuration is automatically accepted. On the other hand, if δC is positive, the new configuration is accepted with a probability that depends on the control parameter T shown in Eq. (16). If a change in configuration is accepted, the projections and $\tilde{o}$ are updated.

At the heart of this method is a thermodynamic analogy to the way liquids crystallize as they cool, ultimately reaching a configuration representing a state of very low energy. Initially, a large value of T is used, so that nearly all changes in configurations are acceptable. Gradually the value of T is reduced and states having a lower energy are favored. Although this algorithm does not guarantee finding a configuration providing the global minimum of the cost function, it is less likely to become "stuck" in a nonglobal minimum since this approach allows the algorithm to "escape" a local minimum in cost with a probability determined by T and the depth of that minimum.

The volume of the region(s) of reconstruction expressed as the number of voxels for which the mask function equals "1" is

$$M = \sum_i \text{mask}(x_i, y_i, z_i). \tag{18}$$

This volume allows 2^M possible distinct binary objects. In addition, it is possible to estimate the total volume, V, in number of voxels occupied by the vessels, from the projection data $p(m,u_j,v_j)$ using densitometry, if signals due to structures other than vessels are removed. If V is held constant, there exists

$$\frac{M!}{V!(M-V)!} (< 2^M \quad \text{for all} \quad V \leq M) \tag{19}$$

distinct objects inside a volume M, determined by the mask function, thereby reducing the number of configurations that need to be investigated.

In order to conserve V in the reconstruction process, changes in configurations of $\tilde{o}$ were performed by turning "on" a single voxel and turning "off" another voxel both located in the masked region. The coordinates $(x_{off}, y_{off}, z_{off})$ give the position of a voxel whose value is changed from 1 to 0 while (x_{on}, y_{on}, z_{on}) is the position of a voxel whose value is changed from 0 to 1. To accelerate the calculations, the cost function is evaluated once for the first estimate of the binary object as shown in Eq. (14), by performing a sum over all detector elements in all of the projections. Thereafter, the change in cost, δC, can be evaluated by updating only the terms in the sum that have been affected by a change in configuration. In this way, for each iteration, differences between the projection of the vessel and the reprojection of the provisional estimate of the vessel are calculated for at most $2l_{max}$ detectors per view. In order to take into account possible overlap in the projections of the two voxels whose values are being changed, δC given by Eq. (2) has been broken into three terms

$$\delta C = \delta C_1 + \delta C_2 + \delta C_3. \tag{20}$$

The first term, δC_1, determines the changes in cost for pixels on the detector affected by the projection of the voxel at $(x_{off}, y_{off}, z_{off})$ only.

$$\begin{aligned} \delta C_1 = \sum_m \sum_{r=1}^{l_{max}} \sum_{s=1}^{l_{max}} \{1 - \delta[u(\alpha_{off},m,r) \\ - u(\alpha_{on},m,s), v(\alpha_{off},m,r) - v(\alpha_{on},m,s)]\} \\ \times \{g[\Delta p_n(m, u(\alpha_{off},m,r), v(\alpha_{off},m,r)) \\ - w(\alpha_{off},m,r)] \\ - g[\Delta p_n(m, u(\alpha_{off},m,r), v(\alpha_{off},m,r))]\}, \end{aligned}$$

where

$$\alpha_{off} = (x_{off}, y_{off}, z_{off}), \tag{22}$$

$$\alpha_{on} = (x_{on}, y_{on}, z_{on}), \tag{23}$$

and

$$\Delta p_n(m,u_j,v_j) = P\{\tilde{o}_n\}(m,u_j,v_j) - p(m,u_j,v_j) \tag{24}$$

is the difference between the projection of the partial reconstruction following the nth iteration and the original projection data. The second term, δC_2, deals with pixels affected by the voxel located at (x_{on}, y_{on}, z_{on}) only.

$$\begin{aligned} \delta C_2 = \sum_m \sum_{r=1}^{l_{max}} \sum_{s=1}^{l_{max}} \{1 - \delta[u(\alpha_{on},m,r) \\ - u(\alpha_{off},m,s), v(\alpha_{on},m,r) - v(\alpha_{off},m,s)]\} \\ \times \{g[\Delta p_n(m, u(\alpha_{on},m,r), v(\alpha_{on},m,r)) + w(\alpha_{on},m,r)] \\ - g[\Delta p_n(m, u(\alpha_{on},m,r), v(\alpha_{on},m,r))]\}, \end{aligned} \tag{25}$$

the third term, δC_3, determines the change in cost for detectors affected by the overlapping projection of both voxels if any.

TABLE I. Values of the temperature parameter kT used in cooling schedules A through D.

	T							
A	400	200	100	70	40	20	10	7
	4	2	1	0.7	0.4	0.2	0.1	
B	400	100	10	1	0.1			
C	400	0.1						
D	0.0001							

$$\delta C_3 = \sum_m \sum_{r=1}^{l_{\max}} \sum_{s=1}^{l_{\max}} \{\delta[u(\alpha_{\text{off}},m,r) - u(\alpha_{\text{on}},m,s), v(\alpha_{\text{off}},m,r) - v(\alpha_{\text{on}},m,s)]\} \times \{g[\Delta p_n(m,u(\alpha_{\text{on}},m,r),v(\alpha_{\text{on}},m,r)) - w(\alpha_{\text{off}},m,r) + w(\alpha_{\text{on}},m,s)] - g[\Delta p_n(m,u(\alpha_{\text{off}},m,r),v(\alpha_{\text{off}},m,r))]\}. \quad (26)$$

The decision whether to accept the new configuration is performed according to the Metropolis algorithm described in Sec. II D. If a change in configuration is accepted, the estimate of the vessel, its projections, and the cost function are updated.

E. Annealing schedule

There is no general rule that can be used to determine the number of "temperature" steps that should be used when performing simulated annealing. The goal is to obtain an optimal solution in the fewest number of iterations possible. Yet it is clear that if the system is not heated or if it is cooled too quickly, a suboptimal solution may be obtained. On the other hand, the use of a large number of temperature steps where the number of iterations per step is fixed might be computationally inefficient since a solution that is nearly as good might have been achieved with far fewer iterations. In Sec. III of this paper, we will investigate how the choice of annealing schedules shown in Table I affects the reconstruction.

In order to determine when to terminate the iteration process, for each value of T, i.e., when thermal equilibrium is reached, an estimate of the variance, σ_C^2, in the cost C, is obtained. Following a change in T, initial estimates of σ_C^2 are large because the cost varies rapidly. As equilibrium is reached, the cost becomes stationary and σ_C^2 approaches a stable value so that differences between consecutive estimates of σ_C^2 decrease. The estimate is calculated for N_{acc} accepted changes in configuration of the object and σ_C^2 is recalculated and compared to its previous estimate. If the current estimate is lower, an additional N_{acc} iterations are performed and the variance is updated. We have selected a value of $N_{\text{acc}}=5000$ to provide a reliable value for σ_C^2. Eventually, differences between consecutive estimates are so small that uncertainties will cause the current estimate to be greater than the previous one. When this happens, a new T value is selected and the process is repeated.

F. Stopping criterion

In order to compare these measures of the effectiveness of our approach, we must also define the criterion that will determine when the reconstruction is stopped. In initial work, the process was terminated when the fraction of misplaced voxels had decreased to a predefined level. However, this approach proved difficult when reconstructing from noisy projection data, because in many instances, this threshold value would never be attained. Therefore, the reconstruction is stopped when the efficiency

$$E = \frac{N_{\text{acc}}}{N_{\text{att}}} \quad (27)$$

which is the ratio of the number of accepted changes in configurations to N_{att}, the number of changes that have been attempted falls below some preset value. This estimate is updated every time 10 000 iterations have been attempted in order to obtain a reliable estimate based on the most recent changes in configuration.

G. Simulations and performance evaluation

The accuracy of a reconstruction from a limited number of projections is a function of numerous factors, including the number of views and their angular distribution, the magnitude of the noise in the image data and the nature of the object being reconstructed. It is not generally possible to obtain analytical expressions describing the effects of these variables on the reconstruction process. As a result, simulations must be performed to assess their influence. In Sec. III, reconstructions of computer-simulated vessel projections are carried out to evaluate the performance of our method.

Evaluation for any particular set of imaging conditions is performed as follows: First, a three-dimensional object is simulated by combining simple geometrical shapes. The image acquisition geometry for each projection is specified and the various discrete cone–beam projections are computed.

The simulations described in Sec. III were performed with

$$\frac{\mathbf{d}}{|\mathbf{d}|} = -\frac{\mathbf{s}}{|\mathbf{s}|}, \quad (28)$$

i.e., the source and the detector are opposite each other with respect to the origin of the coordinates (x,y,z). The distance from the detector to the origin of coordinate $|\mathbf{d}|$ and the distance from the source of the origin of coordinates $|\mathbf{s}|$ are different but constant for all

$$\mathbf{n} = \frac{\mathbf{s}}{|\mathbf{s}|} \quad (29)$$

views. In addition, we require that a normal to the surface of the detector points toward the x-ray source. These constraints were chosen to simulate acquisition about an isocenter. Under these conditions, the acquisition geometry can be specified by the source and detector distance from the isocenter and the angles ϕ and θ as shown in Fig. 5.

The distance between neighboring voxels in the test object and that between adjacent detector elements were chosen to be identical. The reconstructed vessel and original are

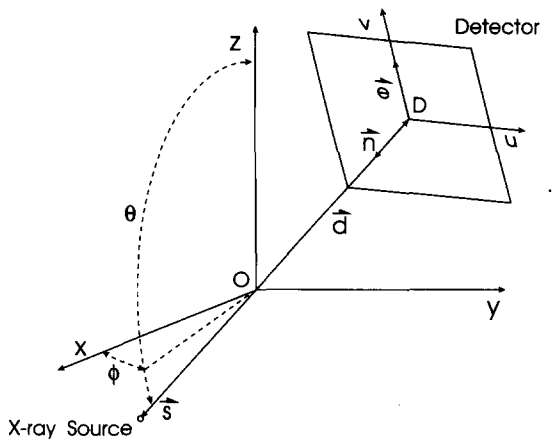

FIG. 5. The acquisition geometry used to project computer-generated binary objects.

viewed using three-dimensional rendering software and compared qualitatively. Then quantitative assessment is performed by determining

$$MV=\left[\left(\sum_i \left\| o(x_i,y_i,z_i)-\tilde{o}(x_i,y_i,z_i)\right\|\right) \Big/ 2\sum_i o(x_i,y_i,z_i)\right]\times 100\% \quad (30)$$

the percentage of voxels having an incorrect value (misplaced voxels). Note that the denominator represents twice the number of voxels having $o(x_i,y_i,z_i)=1$ (i.e., voxels that are part of the original vessel). If the number of voxels in the reconstructed vessel is approximately correct, and $M \geq 2V$, this estimate will have a maximum value of 100%. If $M<2V$ then MV will be less than 100% for the worst possible reconstruction. Normalization by the number of voxels in the vessel is useful when comparing the reconstruction of objects of different sizes.

In some instances, data will be plotted as a function of the normalized cost (NC). This is calculated by dividing the cost C as defined in Eq. (14) by the total number of detector elements that have recorded signal due to vessels in each view.

III. RESULTS AND DISCUSSION

For the purpose of this paper, two simulated discrete binary objects were generated, a sphere having a diameter of 40 voxels cantered on the origin of coordinate x,y,z and a branched vessel exhibiting a stenosis. The principal branch of the vessel has a diameter of 28 voxels. Acquisitions were performed with $|\mathbf{s}|=4000$ voxels and $|\mathbf{d}|=115$ voxels in all cases.

A. Minimization of the cost function

Figure 6 shows both the normalized cost (NC) and the percentage of misplaced voxels (MV) as a function of the number of iterations and temperature parameter T for a spherical object reconstructed from 3 views acquired at

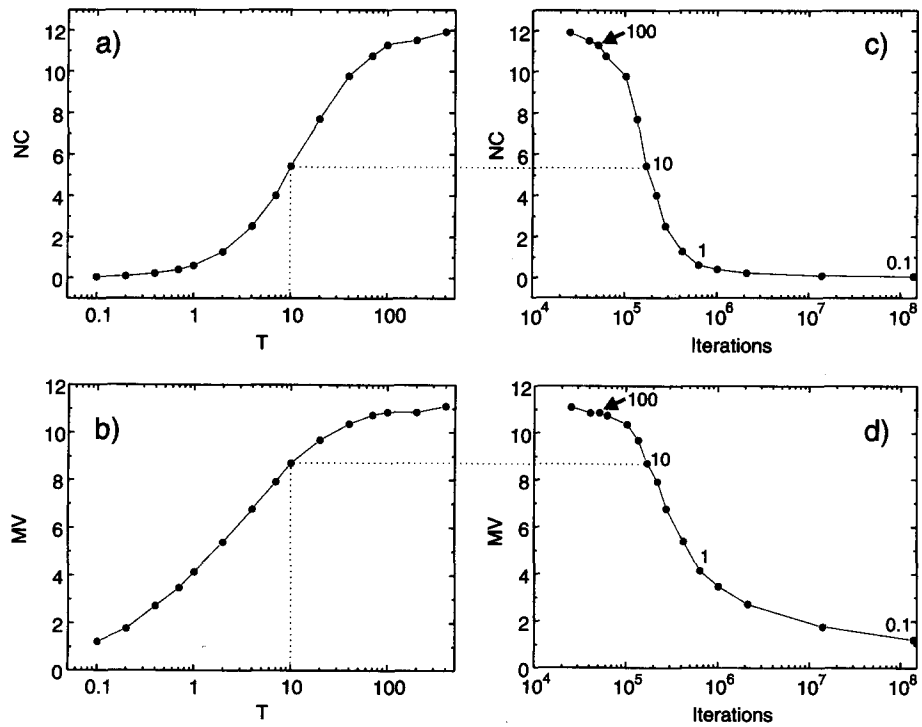

FIG. 6. Minimization of the cost function using simulated annealing. Graphs (a) and (b) show the decrease of the normalized cost (NC) and % misplaced voxels (MV) as a function the temperature parameter T. Graphs (c) and (d) show results of the same simulation as the number of attempted configurations is increased. Values of T are shown for selected points in graphs (c) and (d).

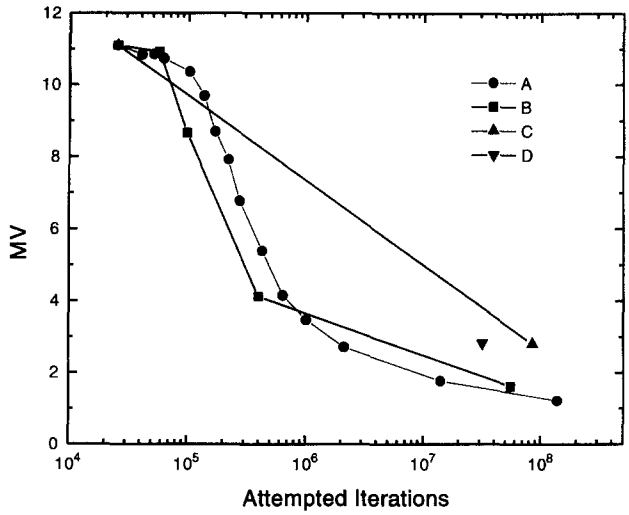

FIG. 7. Graphs depicting the MV as a function of the number of attempted configurations for 4 different cooling schedules described in Table I.

angles (ϕ,θ) of (90,0), (90,60), and (90,120). The points on the graphs were obtained when equilibrium was obtained at a particular value of the temperature parameter T, using cooling schedule A shown in Table I. Figure 6(a) shows that as the temperature is lowered, the NC decreases, indicating improved agreement between the reconstructed image and the projection data. The data also suggest that there is an upper limit of the cost function, so that increasing the value of T beyond 400 should have little effect.

As the cost is minimized (i.e., T is reduced), there is a corresponding decrease in MV as shown in Fig. 6(b). The two curves are similar except that the slope in the "toe" portion of the curve is steeper for MV. The shape of the MV curve suggests that the reconstruction process could have continued with lower T values in order to further improve the accuracy of our results. Since the annealing process involves a number of iterations at each temperature step, values of NC and MV can also be plotted as a function of the cumulative number of iterations performed over all previous and current temperature steps. This is illustrated in Figs. 6(c) and 6(d). Figure 6(d) also shows that as T is lowered, the number of iterations performed at each temperature step becomes prohibitively large as revealed by the relative distances between successive points.

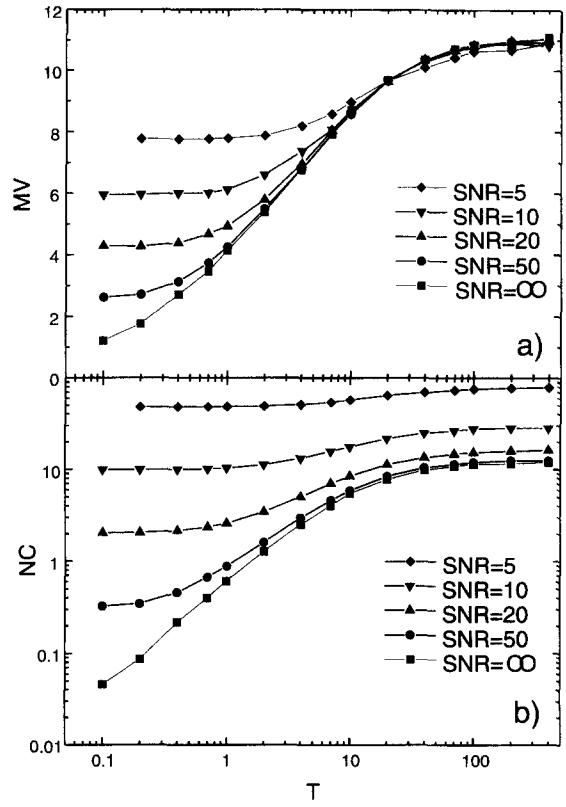

FIG. 8. The percentage of misplaced voxels in (a) and the normalized cost in (b) as a function of T for various SNR values.

B. Annealing schedule

Figure 7 shows how the various annealing schedules described in Table I affect the reconstruction of a sphere using the same acquisition geometry as in the previous simulations. Schedules A, B, and C have the same initial and final values of T, but vary in the number of temperature steps. In all three schedules, the value of T is raised to an initial value to "excite" the system. Schedules A and B yield similar results. In schedule C, the system was quenched through a sudden lowering of the value T, while in schedule D, the initial value of T was not raised but rather lowered at once. These results show that when the temperature is not raised to a high value (as in D) or the system is cooled too quickly (C), the solution obtained is suboptimal as expected. Also, when many temperature steps are used, there is no significant increase in the time required to perform the reconstruction. This occurs be-

TABLE II. Description of geometry used for reconstructions performed with 2, 3, 4, 6, and 9 views.

		View number								
		1	2	3	4	5	6	7	8	9
No.	2	0°,90°	90°,90°							
of	3	0°,90°	60°,90°	120°,90°		ϕ,θ				
views	4	0°,90°	45°,90°	90°,90°	135°,90°					
	6	0°,90°	30°,90°	60°,90°	90°,90°	120°,90°	150°,90°			
	9	0°,90°	20°,90°	40°,90°	60°,90°	80°,90°	100°,90°	120°,90°	140°,90°	160°,90°

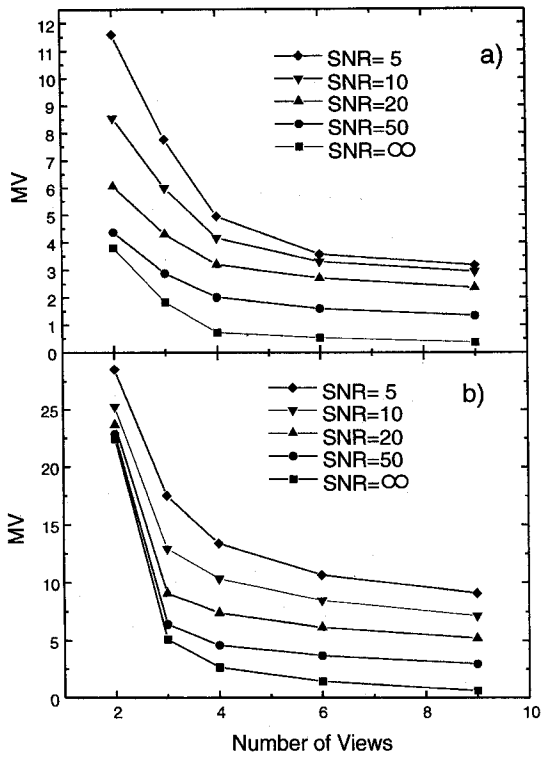

FIG. 9. Graph depicting the percentage of misplaced voxels as a function of the number of views used for various SNR values for (a) a spherical object and (b) a branched vessel.

cause as the difference in temperature between two consecutive steps is reduced, the number of iterations required to reach equilibrium is also lowered. Therefore, it is always better to use a large number of temperature steps and minimize the chances of becoming trapped in a shallow minimum.

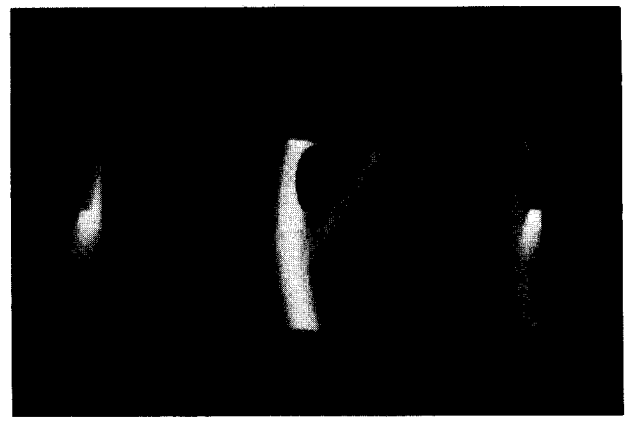

FIG. 10. Projections of a simulated branched vessel exhibiting a stenosis for $(\phi,\theta)=(0,90)$, $(60,90)$, and $(120,90)$.

C. Effect of noise on the annealing process

Gaussian white noise having a spatially independent standard deviation was added to each projection to investigate the effect of signal degradation on the reconstruction. Here, we define the signal to noise ratio (SNR) as the maximum value of $p(m,u,v)$ $\forall$ m,u,v divided by the standard deviation of the gaussian distribution. Figure 8 shows both the NC and MV vs T for different SNR when reconstructing a sphere using the acquisition geometry previously described. These plots show that as the SNR decreases, both the NC and MV

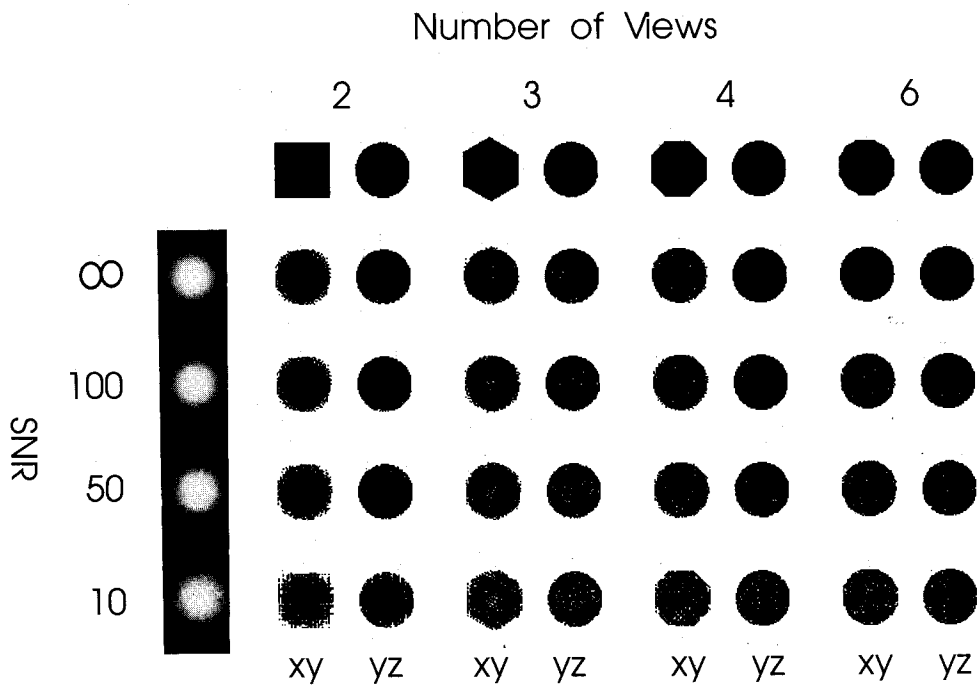

FIG. 11. Diagram showing a cross section through the reconstruction of a sphere in both the xy and yz planes for different SNR and number of views as well as cross sections through the mask function in those same planes (top row). The leftmost column shows projections with different SNR from which the reconstructions were performed.

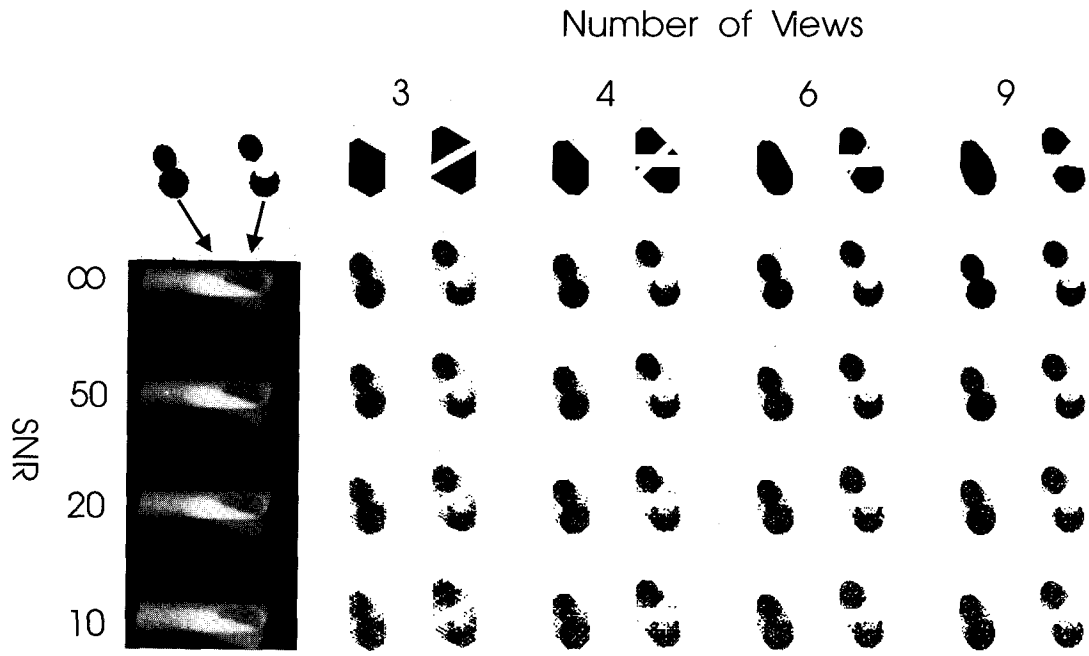

FIG. 12. Reconstructions of the branched vessel. For each SNR and number of views, two cross sections through the xy plane are shown. Two cross sections through the original object are shown in the upper left corner.

curves are shifted toward larger values. Furthermore, as the noise is increased, the temperature above which the curve ceases to be flat increases, so that expending more computing time provides no further improvement in the accuracy of the reconstruction. As a result, the reconstruction process can be safely interrupted sooner in the presence of noise, since little is gained by proceeding to lower values of T.

D. Effect of the number of views on the reconstruction process

The performance of the algorithm was investigated as a function of noise and the number of views. The acquisition geometry for the different number of views used in each simulation is described in Table II. Figure 9(a) shows MV for a sphere as a function of the number of views for different SNR values while Fig. 9(b) gives similar results for a branched vessel with a stenosis. Figure 10 illustrates three projections of this branched vessel. These images show a large vessel with a smaller branch. The narrowing of the large vessel near the bifurcation is evident.

Figure 11 illustrates reconstructions of central sections of the sphere for different number of views and SNR. The first column shows a projection of the object for various SNR values. The top row demonstrates a cross section of the mask

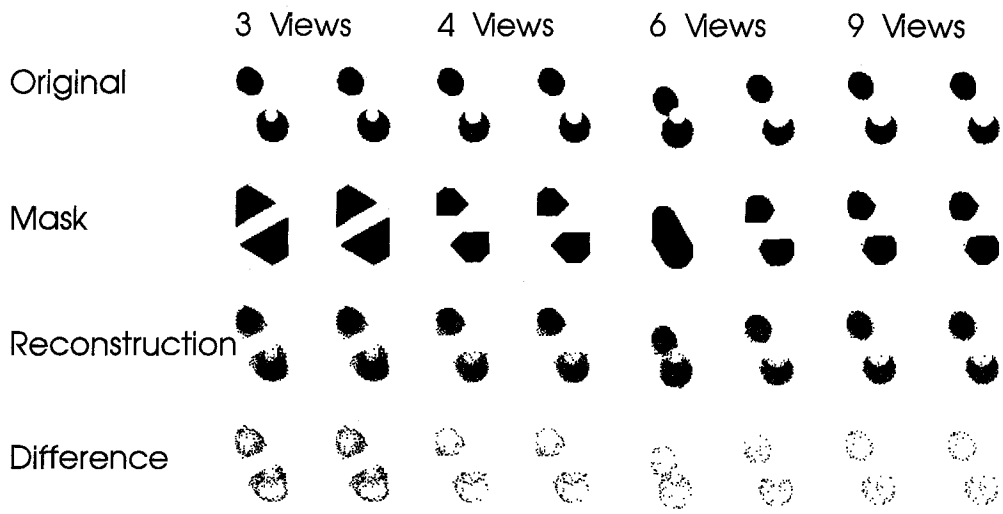

FIG. 13. Diagram showing the most poorly reconstructed slices in the plane of the vessel. Two slices are shown for each number of views. The left slices have more misplaced voxels, while those on the right have a greater fraction of misplaced voxels when normalized by the number of voxels in that slice. In each case, the original cross section, the reconstruction, and their difference are shown.

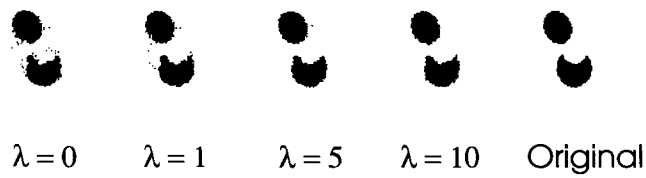

FIG. 14. Reconstructed cross sections in the xy plane of a branched vessel for various values of the continuity parameter λ.

function in both the xy and yz plane for different numbers of views. Cross sections of the reconstructed object in both the xy and yz plane are shown for each SNR and number of views. Figure 11 also reveals that reconstructions in the yz planes are superior to those in the xy plane. This is due to the acquisition geometry used in which all views are acquired by rotating the source in the xy plane. Figure 12 gives similar results for two cross sections in the xy plane through the branching vessel depicted in Fig. 10. These images indicate that better results are achieved when reconstructing a sphere than a more intricate object.

The figure of merit, MV, used to measure the performance of our method so far, was calculated over the whole volume. In order to get a better idea of how the accuracy of the reconstruction will vary from slice to slice, the most poorly reconstructed slices in the plane of the vessel were determined and are depicted in Fig. 13. Two slices are shown for each number of views. Of the two, the leftmost slice has the greater absolute number of misplaced voxels while the slice on the right has the greater fraction of misplaced voxels normalized by the number of voxels in that slice. This second estimate was calculated because the first estimate is likely to be biased toward slices that have many voxels that are part of the vessel. In each case, the true cross section, the reconstruction and their difference are shown. In the difference image, voxels are nonzero only if there is a disagreement between the original and the reconstruction. All reconstructions were performed from projection data having an SNR of 50. The worst slices were located near the ends of the vessels when reconstructing from three or four views. In these slices, the mask function does not constrain the reconstruction very well. Therefore, these slices were excluded from our search for the worst slice in favor of slices that were not reconstructed well due to their more complex nature (stenosis, bifurcations, closely spaced vessels). All of the worst slices shown in Fig. 13 are beyond the bifurcation where the larger branch exhibits a stenosis.

E. Continuity parameter

If a blood vessel is represented as a set of discrete voxels, one notices that in general, a surface can be defined inside of which all voxels will be part of the vessel. As a result, most voxels will have the same values as their closest neighbors except for voxels lying near the lumen boundary. Therefore, it seems reasonable to disfavor a change in configuration that causes a voxel located well inside the lumen of the vessel to change its value to "0" when all of its neighbors have a value of "1." We have begun to investigate whether the addition of a continuity to disfavor such changes can improve the reconstruction. Under such conditions, the expression for the change in cost can be written as

$$\delta C = \delta C_1 + \delta C_2 + \delta C_3 + \lambda[\mathrm{Cont}_{\mathrm{off}}(x_{\mathrm{off}}, y_{\mathrm{off}}, z_{\mathrm{off}}) + \mathrm{Cont}_{\mathrm{on}}(x_{\mathrm{on}}, y_{\mathrm{on}}, z_{\mathrm{on}})]. \tag{31}$$

The variable λ is a parameter that weighs the contribution of the continuity functions. The continuity term increases the value of δC when a change in configuration that fragments the object is attempted, making it less likely that such a modification will be accepted.

The function

$$\mathrm{Cont}_{\mathrm{off}}(x_i, y_i, z_i) = \begin{cases} \sum_{l,m,n=-1}^{1,1,1} \tilde{o}(x_i + l\Delta x, y_i + m\Delta y, z_i + n\Delta z) - \tilde{o}(x_i, y_i, z_i) - 18 \\ \qquad \text{if} \quad \sum_{l,m,n=-1}^{1,1,1} \tilde{o}(x_i + l\Delta x, y_i + m\Delta y, z_i + n\Delta z) - \tilde{o}(x_i, y_i, z_i) \geq 18 \\ 0 \quad \text{otherwise} \end{cases} \tag{32}$$

has a minimum value of 0 when fewer than 19 of the 26 nearest neighbors have a value of "1" (i.e., more than 7 have a value of "0") and increases to a maximum value of 8 when all 26 closest voxels have a value of "1." The variables Δx, Δy, Δz are the dimensions of the voxels. This function is used to prevent a voxel within the lumen from being turned off. The function

$$\mathrm{Cont}_{\mathrm{on}}(x_i, y_i, z_i) = \begin{cases} 8 - \sum_{l,m,n=-1}^{1,1,1} \tilde{o}(x_i + l\Delta x, y_i + m\Delta y, z_i + n\Delta z) + \tilde{o}(x_i, y_i, z_i) \\ \qquad \text{if} \quad \sum_{l,m,n=-1}^{1,1,1} \tilde{o}(x_i + l\Delta x, y_i + m\Delta y, z_i + n\Delta z) - \tilde{o}(x_i, y_i, z_i) \leq 8 \\ 0 \quad \text{otherwise} \end{cases} \tag{33}$$

takes on a value of 0 when fewer than 19 of the 26 nearest neighbors have a value of "0" and increases to a maximum value of 8 when all 26 closest voxels have a value of "0." This function increases δC when one attempts to turn on a voxel far from the lumen.

Figure 14 illustrates the reconstruction of a branched vessel from 3 projections having a SNR of 50, for different values of the parameter λ ($\lambda=0$ indicates that the continuity correction is not applied). The acquisition geometry can be found in Table I. As λ is increased, we note that the reconstruction improves. Our results show that significant reductions in the MV from 9% to 4% can be achieved in this instance. However, the way in which the continuity function was defined is based on results from a limited number of simulations and is somewhat arbitrary. Further work will be required to determine if our approach is an effective way to impose continuity conditions. A better strategy than just adding a new term to the cost function might be to restrict the initial attempts at configuration changes to the lumen boundary, reducing the number of configurations that are attempted, and possibly reducing the time required to perform the reconstruction. The results obtained thus far warrant further investigation.

IV. CONCLUSION

Our results demonstrate that it is possible to reconstruct a simulated branched vessel exhibiting a stenosis with as few as 4% of voxels misplaced using three views with a SNR >50. This performance is realized through the introduction of "binarity" and continuity constraints into the reconstruction. These constraints could not be introduced into an iterative reconstruction method and as a result the reconstruction process was treated as a large scale minimization problem and solved using simulated annealing. This approach results in a large number of computations so that the reconstruction of the branched vessel shown in this paper required several hours.

Since our method was verified by creating simulated three-dimensional objects (mathematical abstractions) from which projections were calculated, no subtractions of signals due to structures other than blood vessels were necessary. In order to apply this method to real angiographic projections, it will be necessary to isolate vessels in each projection and perform other corrections (geometric distortions, misregistration). These issues will be addressed in a future paper where this method will be applied to iodinated vessel phantoms.

ACKNOWLEDGMENTS

The authors wish to acknowledge the support of the Heart and Stroke Foundation of Canada as well as the Fonds pour la Formation de Chercheurs et l'Aide à la Recherche du Québec.

[1]T. A. DeRouen, J. A. Murray, and W. Owen, "Variability in the analysis of coronary arteriograms," Circulations **55**, 324–328 (1977).

[2]L. M. Zir, S. W. Miller, R. E. Dinsmore, J. P. Gilbert, and J. W. Harthorne, "Interobserver Invariability in Coronary Angiography," Circulation **53**, 627–632 (1976).

[3]K. M. Detree, E. Wright, M. L. Murphy, and T. Takaro, "Observer Agreement in Evaluating Coronary Angiograms," Circulation **52**, 979–986 (1975).

[4]B. G. Brown, E. Bolson, M. Frimer, and H. T. Dodge, "Quantitative coronary angiography. Estimation of dimensions, hemodynamic resistance, and atheroma mass of coronary artery lesions using arteriogram and digital computation," Circulation **55**, 329–337 (1977).

[5]K. L. Gould and R. L. Kireeide, "Assessment of stenosis severity," in *State of the Art in Quantitative Arteriography*, edited by J. H. C. Reiber and P. W. Serruys, (Dordrecht, Nijhoff, 1986), pp. 209–228.

[6]J. H. C. Reiber *et al.*, "Assessment of short- medium- long term variation in arterial dimensions from computer assisted quantitation of coronary angiograms," Circulation **71**, 280–288 (1985).

[7]A. B. Nichols, C. F. O. Gabrieli, J. J. Fenoglio, and P. D. Esser, "Quantification of relative coronary arterial stenosis by cinevideodensitometric analysis of coronary arteriograms," Circulation **69**, 512–522 (1984).

[8]K. R. Hoffman, Kunio Doi, Heang-Ping Chan, and Kok-Gee Chua, "Computer reproductions of the vasculature using an automated tracking method," Proc. SPIE **767**, 449–453 (1987).

[9]C. Smets, G. Verbeeck, P. Suetens, and A. Osterlinck, "Knowledge-based delineation of coronary angiograms," in *Signal Processing, IV: Theories and Applications*, edited by J. L. Lacoume, A. Chehikian, N. Martin, and J. Malbos (North-Holland, Amsterdam, 1988), pp. 1259–1262.

[10]D. L. Parker, D. L. Pope, R. Van Bree, and H. W. Marshall, "Three-Dimensional Reconstruction of Moving Arterial Beds from Subtraction Angiography," Computers and Biomed. Research **20**, 166–185 (1987).

[11]S. K. Chang, "The Reconstruction of Binary Patterns from their Projections," Communications of the ACM **14**, 21–26 (1971).

[12]G. M. Mawko and T. M. Peters, "Iterative 3-D reconstruction of vascular images from a few views: Phantom study result," in *Proc. SPIE Physics and Engineering of computerized multidimensional imaging and image processing* **671**, 19–24 (1986).

[13]J. A. Högbom, "Aperture synthesis with a nonregular distribution of interferometer baselines," Astron. Astrophys. Suppl. **15**, 417 (1974).

[14]R. M. Rangayan and R. Gordon, "Streak preventive image reconstruction with ART and adaptive filtering," IEEE Trans. Med. Imag. **MI-1**, 173–178 (1986).

[15]J. R. Spears, T. Sandor, R. Kruger, W. Hanlon, S. Paulin, and G. Minerbo, "Computer reconstruction of luminal cross sectional shape from multiple cineangiographic views," IEEE Trans. Med. Imag. **MI-2**, 49–54 (1983).

[16]G. Minerbo, "A maximum entropy algorithm for reconstructing a source from projection data," Computer Graphics and Image Processing **10**, 48–68 (1979).

[17]S. K. Chang and C. K. Chow, "The reconstruction of three dimensional objects from two orthogonal projections and its application to cardiac angiography," IEEE Trans. Comp. **C-22**, 18–28 (1973).

[18]S. K. Chang and Y. R. Wang, "Three-dimensional object reconstruction from orthogonal projections," Pattern Recognition **7**, 167–176 (1975).

[19]Y. R. Wang, "Characterization of binary patterns and their projections," IEEE Trans. Comp. **C-24**, 1032–1035 (1975).

[20]C. H. Slump and J. J. Gerbrands, "A network flow approach to the reconstruction of the left ventricle from two projections," Comput. Graph. Image Processing **18**, 18–36 (1982).

[21]J. H. C. Reiber, J. J. Gerbrands, G. J. Troost, C. J. Kooijman, and C. H. Slump, "3D reconstruction of coronary arterial segments from two projections," in *Digital Imaging in Cardiovascular Radiology*, edited by P. H. Heintzen and R. Brennecke (Georg Thieme Verlag, New York, 1983), pp. 151–163.

[22]L. Van Tran, R. C. Bahn, and J. Sklansky, "Reconstructing the cross sections of coronary arteries from biplane angiograms," IEEE Trans. Med. Imaging **11**, 529 (1992).

[23]A. Schliferstein and Y. T. Chien, "Switching component and the ambiguity problem in the reconstruction of pictures from their projections," Pattern Recognition **10**, 327–340 (1978).

[24]A. V. Crewe and D. A. Crewe, "Inexact reconstructions from projections," Ultramicroscopy **12**, 293–298 (1984).

[25]A. V. Crewe and D. A. Crews, "Inexact reconstruction: Some Improvements," Ultramicroscopy **16**, 33–40 (1985).

[26]S. Krishnan, S. S. Prabhu, and E. V. Krishnamurthy, "Probabilistic reinforcement algorithms for the reconstruction of pictures from their projections," Intern. J. Systems Sci. **4**, 661–670 (1973).

[27]P. Suetens, A. Haegemans, A. Oosterlinck, and J. Gybels, "An attempt to

reconstruct the cerebral blood vessels from a lateral and a frontal angiogram," Pattern Recognition **16**, 517–524 (1983).

[28]R. Gordon, R. Bender, and G. T. Herman, "Algebraic reconstruction technique (ART) for three-dimensional electron microscopy and x-ray photography," J. Theor. Biol. **29**, 471–481 (1970).

[29]S. Kirkpatrick, C. D. Gelatt, and M. P. Vechi, "Optimization by simulated annealing," Science **220**, 671–680 (1983).

[30]N. Metropolis, A. Rosenbluth, M. Rosenbluth, A. Teller, and E. Teller, "Equation of state calculation by fast computing machines," J. Chem. Phys. **21**, 1087–1092 (1953).